J Mater Sci (2010) 45:688–700
DOI 10.1007/s10853-009-3986-6

Cyclic oxidation and wear of tungsten rods in contact with glass in atmospheric air

C. Dorgans · J.-M. Chaix · L. Boulangé · Y. Bréchet

Received: 1 July 2009 / Accepted: 13 October 2009 / Published online: 29 October 2009

Abstract Tungsten tools used in the glass-forming industry undergo complex damage process resulting from cyclic contact with molten glass and atmospheric air and from friction between glass and tungsten. The damage process involving oxide scale growth and wear has been studied on W rods of two different diameters, in contact or not with glass, with different friction velocities. Damage is characterized quantitatively and the contributions of oxidation, borosilicate glass–tungsten reaction, and wear are discussed.

Introduction

Some tungsten tools are used in glass-forming engineering at high temperature (up to 1000 °C) in air. Under these conditions, tungsten is expected to undergo oxidation by air and chemical interactions with glass. At the W–glass interface, the shear stresses coming from the relative motion of W and glass during the forming process can lead to wear. It is therefore important to analyze, quantify, and understand tungsten damage under glass-forming conditions.

Between room temperature and 1000 °C, tungsten is known to be oxidized in air [1, 2]. All authors report on the formation of a double-layer scale composed of a thin adherent dark protective layer and a yellowish porous layer [3–7]. However, the oxidation kinetics established are not always the same. Some authors find linear oxidation rate [8], others parabolic [4], and others claim to find a kinetic law which is neither linear nor parabolic [3, 7]. The two oxides layers are assumed to have different compositions [4, 6, 7] or different structural perfection or orientation [5]. Tungsten oxides can volatilize [8, 9] above 800 °C. Steam [10, 11] seems to increase the volatilization of the oxides. It is fairly well established [4] that high temperature oxidation of tungsten is sensitive to: diffusion processes involving the formation of defects and the diffusion of metal or oxygen atoms through the oxide scale, heat effects associated with oxidation, desorption or evaporation of WO_3. Adhesion of the oxide scale to the metal at the surface and at the specimen edges [4] as well as cold or hot shearing [3, 4, 8] have an effect on the kinetics of tungsten oxidation. Shearing, for instance, produces an exfoliation of oxides [3, 4, 8] and limits their protective character.

In addition to oxidation aspects, glass-forming operations involve shear stresses at the metal/glass surface. These stresses may damage and remove the oxide layer and thus, wear and oxidation are expected to have a synergetic effect. In order to study this effect, the tungsten samples investigated are cylindrical rods rotating at a prescribed angular velocity. Two rod diameters are investigated, corresponding to two tangential velocities. The contact conditions between the molten glass and the rod, due to different temperatures and types of contact with air or molten glass, produce differences between the samples in particular in terms of oxide scale and wear rate.

The involved wear process differs from the ones usually encountered in recent studies, which aim at improving wear resistance of metals worn by another solid, with [12] or without [13] surface treatments or protected by oxide layers [14]. In the present study, the oxide scale is formed and worn at high temperature by a viscous fluid (glass).

The contact situations between tungsten, air, and molten glass raises some questions about the chemical nature of the oxide layer. Which tungsten oxide WO_x is formed? Does the presence of glass lead to mixed oxides such as

C. Dorgans (✉) · J.-M. Chaix · L. Boulangé · Y. Bréchet
SIMaP, Grenoble INP-CNRS-UJF, BP75, 38402 Saint Martin d'Hères, France
e-mail: celine.dorgans@simap.grenoble-inp.fr

tungsten bronzes? Which mechanisms are involved and which ones predominate? The chemical stability of the formed oxides is important for the evolution of the tungsten sample. The mechanical stability of the oxide layer is also an issue: are the stresses due to oxidation (Pilling–Bedworth ratio is 3.3 [3]) and the stresses due to differential thermal dilation during cycling able to lead to exfoliation of the oxide scale? Do the shear stresses due to rotation at the glass–oxide interface play a major role in the wear damage?

The aim of this article is to understand the mechanisms of oxidation involved in the cyclic process when tungsten interacts directly or not with glass. The diameter evolution, the oxide morphology, and the chemical composition of tungsten samples were analyzed before and after use during different numbers of cycles.

Materials and experimental methods

Tungsten samples and glass

The tungsten samples are cylinders cut from wires drawn from a powder metallurgy bulk product of tungsten with a purity of 99.95%. The main impurities were iron and molybdenum.

Two diameters were studied: 500 μm ("large diameter") corresponding to as-drawn wires, and 250 μm ("reduced diameter") obtained from machined cylinders. The scratches observed on large diameter rods (Fig. 1a) result from the wire drawing; the traces of machining process are observed on machined parts of small cylinders (Fig. 1b).

A borosilicate glass was used to study the cyclic oxidation and wear of the tungsten samples. The chemical composition of the glass and its physical properties are summarized in Table 1.

Experiments

Samples are held in a metallic holder at room temperature. The rods rotate at constant velocity and they are cyclically put in contact with hot glass (Fig. 2) at about 1000 °C. The tungsten sample initially at holder temperature is inserted inside the glass. After staying a while in the glass, the sample is removed. Each cycle lasts less than 2 s and is repeated hundreds of times.

The geometry of the glass bath is a shell of about 2-mm thick which is punched through by the wire. The tungsten sample is alternatively at high temperature (between 800 and 1000 °C) and low temperature (below 400 °C). It is only heated by the hot glass and cooled by air at room temperature and through the sample holder. Temperatures given in this article are those measured on glass by pyrometry.

Since tungsten samples and glass are rotating with respect to each other along the cylinder symmetry axis with a relative velocity of the order of m/min, the outside surface of the tungsten sample is undergoing friction with glass. An additional friction, parallel to the axis, occurs when the tungsten sample is withdrawn from glass. These

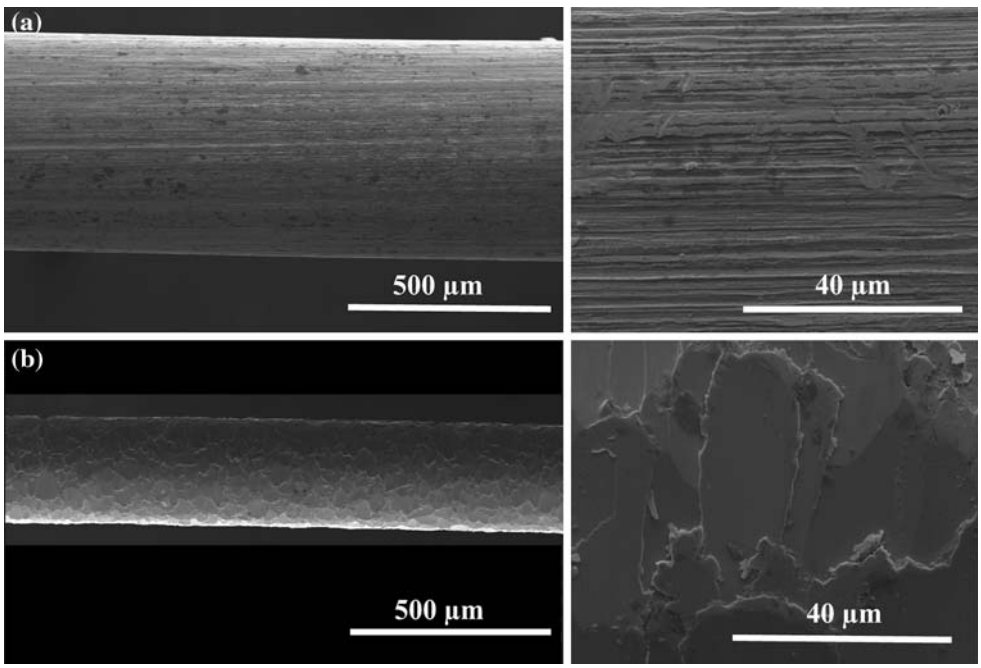

Fig. 1 SEM images of the tungsten samples (20 kV, WD = 10 mm, SE mode) before use. The *scratches* observed on large-diameter samples (**a**) are characteristic of the drawing and the *traces* seen in small-diameter samples (**b**) are characteristic of the machining

Table 1 Chemical composition and physical properties of glass

Chemical composition (wt%)		Physical properties		
SiO_2	74.5	Glass transition T_g (°C)		520
B_2O_3	10.4	Glass temperature at viscosity η in dPa.s	10^{13} (annealing point) (°C)	566
Al_2O_3	6		$10^{7.6}$ (softening point) (°C)	779
$Na_2O + K_2O$	8.3		10^4 (working point) (°C)	1144
BaO	<0.05	Density at 25 °C (g cm^{-3})		2.33
CaO + MgO	0.5	Mean linear thermal expansion α(20, 300 °C) according to ISO 7991		5.1×10^{-6} K^{-1}
F_2, Cl_2, Fe_2O_3, MnO_2, Li_2O	0.3			

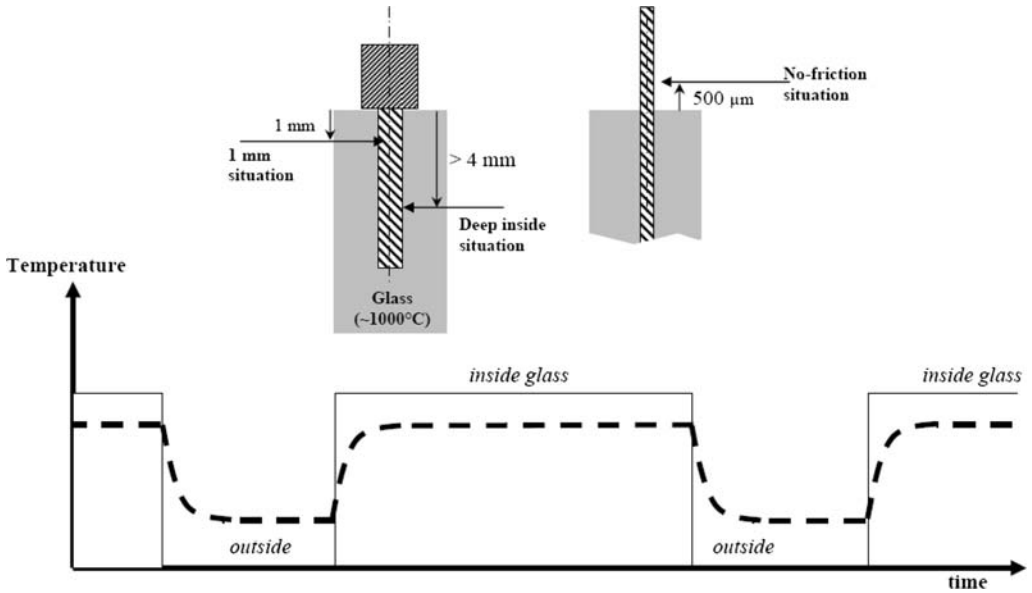

Fig. 2 Schematic view of the cyclic oxidation and wear experiment on tungsten samples. The tungsten rods are alternatively outside and inside the glass and heated by it. During the hot stage, tungsten in the "no-friction situation" is outside the glass but is submitted to a hot glass atmosphere, the "deep inside situation" corresponds to contact with the glass in the hottest zone, and the "1 mm situation" also corresponds to contact with the glass but close to the metallic holder and at lower temperature. The cyclic thermal and contact conditions are schematized in the *bottom* of the figure

mechanical loadings are mainly applied while the sample temperature is high (above 800 °C). The use of two different wire diameters allows to monitor these shear components.

Two positions on the tungsten rod are considered in this article (Fig. 2):

- "1 mm situation", 1 mm inside the glass, is close to the steel holder which acts as a heat sink so that tungsten is expected to reach a lower temperature for the hot stage; the contact with glass is also slightly shorter. This situation was only studied for large cylinders. This point is located far enough from the steel holder to prevent from considering the presence of iron in the oxide scale. Iron was only detected in the oxide scale for a distance closer to the steel holder (less than 500 µm).
- "Deep inside situation", more than 4 mm inside the glass, where tungsten is assumed to get the same temperature as glass (about 1000 °C) during the hot stages. This situation is studied for small and large diameters.

Shear stresses on the oxide layer are expected to be different for the large and small diameters, as the relative velocities of the glass and the sample are different. The average temperature along the hot stage of each cycle is likely to be higher for the small-diameter rods due to a lower thermal inertia and for a position further apart from the metallic holder which probably acts as a heat sink.

The third situation is studied as a reference for cyclic oxidation of tungsten not submitted to friction. This "no-friction situation" is close to the glass surface. In these conditions, the temperature is expected to be close to the glass one, as for the "deep inside situation". This situation involves a "hot glass atmosphere" of air potentially containing volatile glass components. It is also relevant of

glass-forming process situations. Experimentally, this corresponds to 500 μm above the glass surface in a long rod which is partly inserted in the glass bath (Fig. 2).

In this article, the damage was evaluated on tungsten samples with increasing number of thermomechanical cycles.

Environmental scanning electron microscope observation methods

A Quanta 400 Environmental Scanning Electron Microscope (ESEM) by FEI (Lyon, France) was used, with 20-kV high tension and 10-mm working distance, using both Secondary Electron (SE) and Back Scattered Electron (BSE) modes, when necessary, to improve the interpretation of images. Views at low magnification (×100) were used to get an overview and higher magnification (×2,000) was used to identify typical microstructures in the different situations. Low magnification, highly contrasted BSE images were used to measure the apparent variation of diameter.

Axial (longitudinal) sections of the samples were prepared. The tungsten samples, embedded in Varidur 3000 (Buehler, Dardilly, France) methacrylate-styrol cold mounting resin, were polished parallel to the axis with grade 80 to 600 SiC papers. Polishing was finished with 2500 SiC paper and 6-, 3-, and 1-μm diamond paste. The sections were observed by SEM in the same conditions as above.

Energy dispersive X-ray analysis procedures

O, Na, Si, Ca, and W were analyzed on images at magnification ×2,000 by EDX semi-quantitative analysis in the ESEM using an Oxford Inca probe. Boron was not analyzed because this light element could not be efficiently detected. Reference standards were used to perform the evaluation: orthoclase standard for O, jadeite standard for Na, SiO_2 standard for Si, orthoclase standard for K, Wollastonite standard for Ca, and W standard for W. Values below twice the standard deviation were set to zero, the sum of weight percents of element being set to 100%, and only three iterations were used by the software to give a weight percentage. In the case of axial sections, higher magnification was used (×80,000) and Si, not detected in the scale but present in the embedding resin, was removed from the fixed element list.

X-ray diffraction methods

X-ray diffraction was carried out at room temperature using a PanAlytical X'Pert Pro MPD with CuKα radiation in a Θ–Θ configuration. A series of identical samples of large diameter samples for the "1 mm situation" and the "deep inside situation" were put side by side to form a raft with a surface of 1 mm^2. Phase identification of the sample surface was carried out with the PDF-2 database from the International Centre for Diffraction Data (ICDD).

Results

Macroscopic approach

Macroscopic observations of the samples before and after a sequence of immersion emersion in the glass were performed with ESEM at low magnification (×100). Measurements of apparent diameter variation after various numbers of cycles were performed along the samples, and average values were calculated for the different situations (Fig. 3). The diameter evolution in the different situations

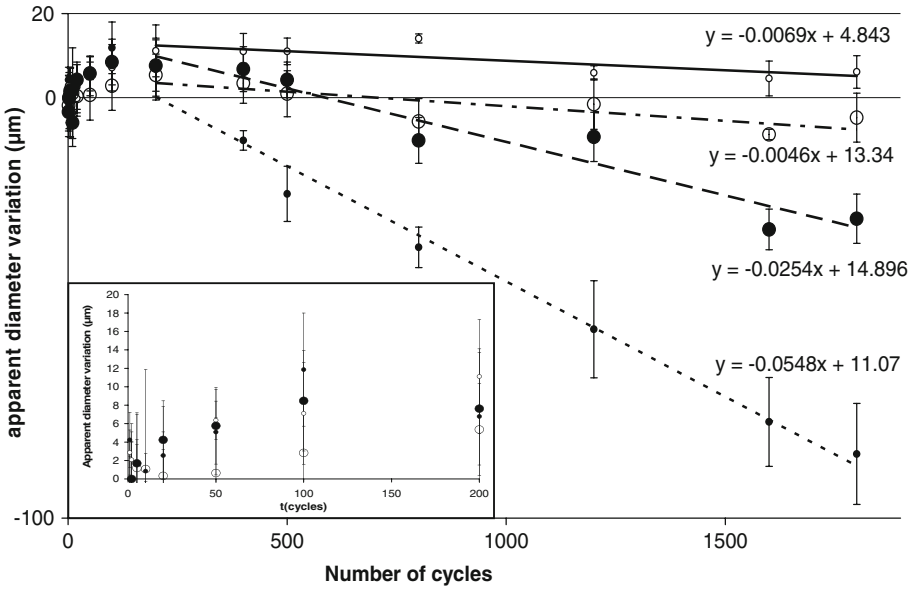

Fig. 3 Evolution of the apparent diameter variation with the number of cycles for the considered situations: "no-friction" (*small empty marks*), "deep inside" glass with small diameter (*small full marks*), "deep inside" glass with large diameter (*large full marks*), "1 mm" inside glass (with large diameter) (*large empty marks*). In the *inset*, the zoom in for the 200 first cycles is presented

is similar: the diameter first increases during 50–100 cycles, then decreases. However, the amplitude of the variation depends on the considered situation. The first increase, which can be roughly associated to oxide formation, is almost similar in the "no-friction" and in the "deep inside" situations, but significantly slower in the "1 mm situation". The decrease in diameter, which can be mainly associated to wear, is more significant in the "1 mm situation" and the "deep inside situation" in which the tungsten rod is rotating in contact with the glass. Diameter steeply and linearly decreases in the "deep inside situation", with a rate of 0.055 μm/cycle for small-diameter and at about half this rate (0.025 μm/cycle) for large-diameter rods. The diameter decreases less in the "1 mm situation", and the apparent variation diameter also becomes negative for large numbers of cycles. A very small decrease after 10 cycles in the "no-friction situation" is however observed, the apparent variation of diameter remaining positive.

External morphology of the reaction layer

Observations of the oxides scale after different number of cycles are illustrated in Fig. 4. In the first ten cycles, the initial surface morphology of drawn and machined samples is still seen. In these first cycles, a granular layer is observed at the surface of the samples. This coverage is continuous and homogeneous in the "no-friction situation", contrary to the other ones. After 50 cycles, the oxide scale depth is large enough to hide the initial surface state in all cases, and the scale surface appears granular, with strong differences in the nature and arrangement of constitutive grains:

- In the "no-friction situation", an external layer of grains grows until 800 cycles with a microstructure composed of isotropic and anisotropic features. Depending on the observed area, these objects can be related by a cement-like phase, or separated by some porosity at the grain boundaries. They look like rounded crystals and appear either isotropic or elongated. This observation can correspond to two types of objects or to platelets observed from different orientations. The typical dimension of the isotropic objects is about 1 μm for 50 cycles, 1.5–2 μm for 100 cycles, 3 μm for 400 cycles, and almost stabilized to about 5 μm above 800 cycles. The typical dimension of the elongated objects, whichever the number of cycles, is 1-μm thick and 5-μm long. Above 1,200 cycles, long inter- and intra-granular cracks are observed.
- In the "deep inside situation", for small-diameter rods, the microstructure behavior after 50 cycles is drastically different when compared to the "no-friction situation". The first observation is that the characteristic feature size is almost constant, and much smaller than in the "no-friction situation". The microstructure is constituted by isotropic, elongated, and fragmented objects, these last ones being isotropically oriented. In addition, anisotropic objects that seem to be deposited on the surface are seen. Large cracks can be observed even after 100 cycles. Above 400 cycles, isotropic objects are no longer seen and thin anisotropic objects of about 1-μm width and 3-μm length are seen again.
- The "1 mm situation" and in the "deep inside situation", for large diameters, exhibit a common behavior, with different kinetic rates. The growth of isotropic and elongated (randomly oriented) objects is observed until some apparent stabilization sets in. The growth in these situations appears slower than for small rods in the "deep inside situation", and reaches sizes which are three to five times smaller. The growth was quicker in the "deep inside situation" than in the "1 mm" one. As in the "no-friction situation", porous and cemented areas are observed. A significant amount of the surface is covered by grains that appear as issued from the fragmentation of large objects into irregular lamellae. The typical dimension of the fragmented objects is about 5–10 μm and the isotropic objects size and lamellae width is about 1–2 μm.

Above 100 cycles, isolated isotropic pores could be observed in all situations, in addition to the cracks, fragmented objects, and porosity at grain boundaries. Although the presence of a glass thin layer was considered that could have disturbed the observations, no presence of glass could be evidenced on the oxide layer surface by ESEM observations and EDS analyses.

Axial cross section of the layer

Axial cross sections of the scale after 1,800 cycles show a thicker scale in the "no-friction situation" than in the other ones (Fig. 5). This is in good agreement with the apparent variation of diameter measured as a function of time illustrated in Fig. 3.

In all cases, the oxide scale is constituted by two layers (Fig. 5), an inner compact one at the metal surface and an outer layer. An extra layer is also seen in the case of the small diameter for the "deep inside situation". The inner compact layer is similar in all cases and typically 4–5-μm thick. The tortuous interface between oxide and metal (also observed by Webb et al. [7]) suggests the occurrence of a grain-boundaries-enhanced oxidation.

The outer layer differs from one situation to another. In the "no-friction situation", it is composed of large crystals, with a size gradient from smaller inner ones to larger outer ones, which corresponds to the objects

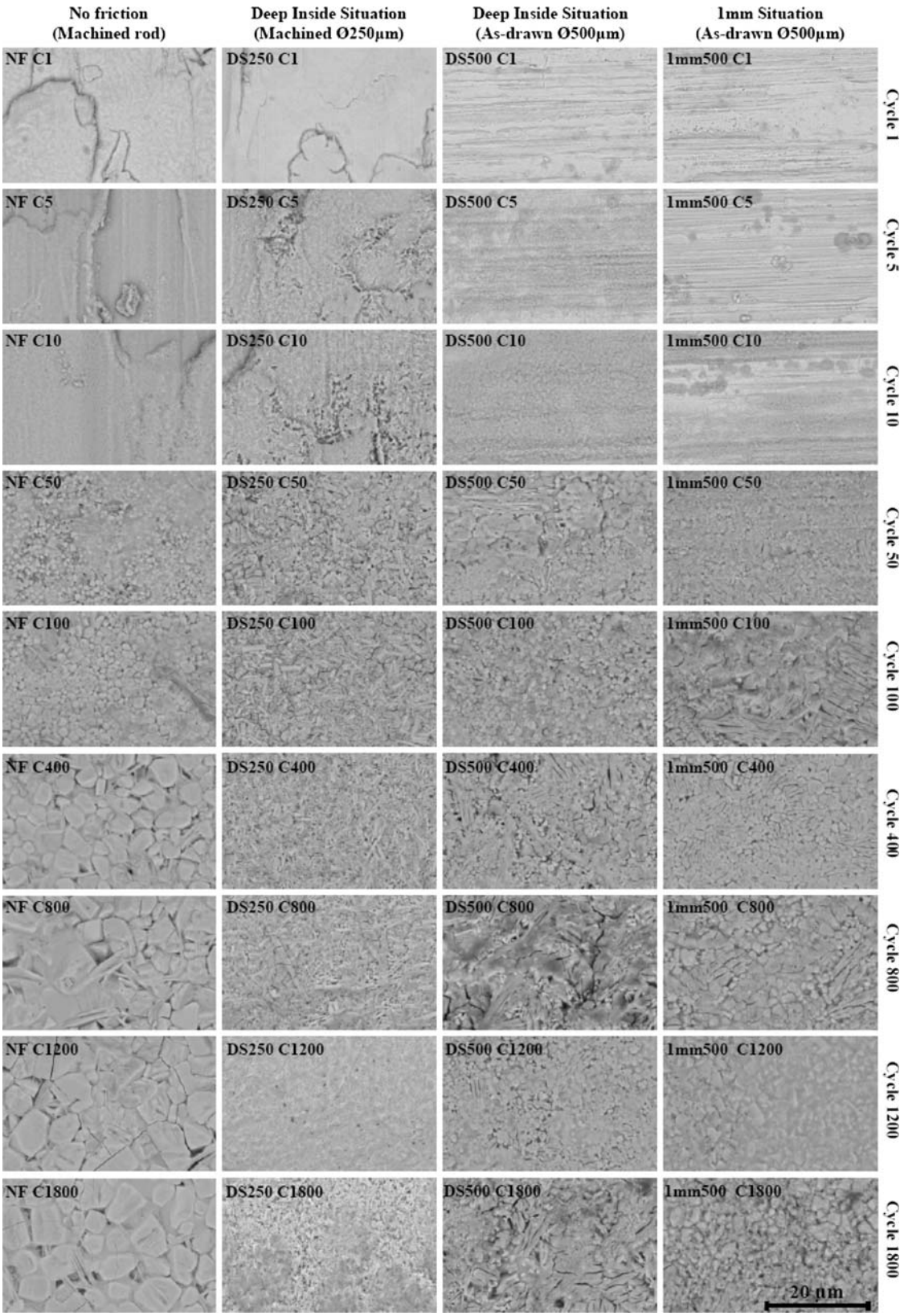

Fig. 4 External evolution of the oxide scale morphology after 1–1,800 cycles, for the different situations: top observation by SEM (20 kV, WD = 10 mm, BSE mode)

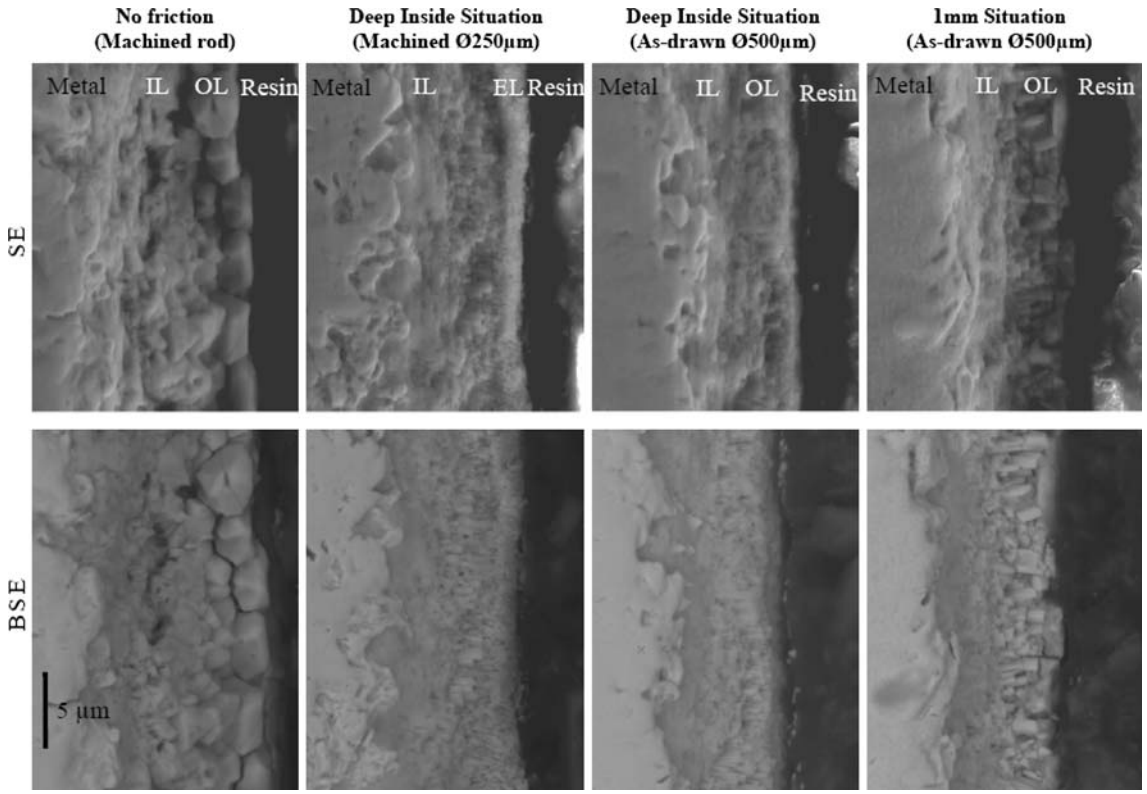

Fig. 5 Cross sections of the oxide scale parallel to the sample axis after 1,800 cycles. Two layers are observed, an inner one (IL), and an outer one (OL); in the "deep inside situation" for small diameter, an extra-layer (EA) is observed (SE and BSE SEM pictures, 20 kV, WD = 10 mm)

observed on Fig. 4 (image NF C1800). Large grains slightly wider (5 µm) than thick (2–3 µm) form the outer pavement of the scale. A similar gradient in the microstructure is observed in the "1 mm situation", but with smaller crystals (3-µm high and 1-µm width). This feature is reminiscent of a columnar growth in which objects would have been broken. On the top of this outer layer, some cracked objects of more than 5-µm long are present and are reminiscent of the fragmented objects seen in the friction situations on Fig. 4. In the small-diameter samples in the "deep inside situation", this columnar growth is also seen in the outer layer, but an extra layer is present. This almost compact layer seems to be composed of thin anisotropic objects deposited on the outer layer. It was not systematically observed when observations were repeated in the same situation.

Elementary analysis of the top of the scale

Elementary analysis of the top of the scale was performed with EDX as a function of the number of thermomechanical cycles. The atomic percentage of tungsten is presented in Fig. 6 as well as the evolution of atomic ratios of oxygen, sodium, calcium, and potassium to tungsten. The level of W in the scale decreases until 50 cycles, while the level of oxygen increases, then both of them stabilize. This is probably the number of cycles to get an oxide scale thick enough to prevent from the detection of the metal below the scale. Above 50 cycles, data are obtained from an external region of the oxide scale, typically 1–2 µm.

Sodium is present at a relatively high level (Na/W = 0.4–0.6) in friction situations, with a plateau similar to that of oxygen above 100 cycles. In the "no-friction situation", the amount of sodium remains significantly lower (Na/W = 0.1–0.2). Almost the same observations are valid for potassium, with plateau values about 15 times lower and consequently large fluctuations in the data. Calcium was not detected in all situations. It is present in the "1 mm situation" (Ca/W = 0.05–0.1) and at very low level (Ca/W = 0.01) in the "deep inside" one for large diameter.

The data (Table 2) and histogram of average plateau values (Fig. 6) indicate a mean composition of oxide $Na_xK_yCa_zWO_i$ in each case. In the "no-friction situation", the layer mainly contains W, Na, and O, and appears to have, in the accuracy limits of the present semi-quantitative analysis, the lowest O content of all situations. In the same limits, the value of O/W above 3 in friction situations

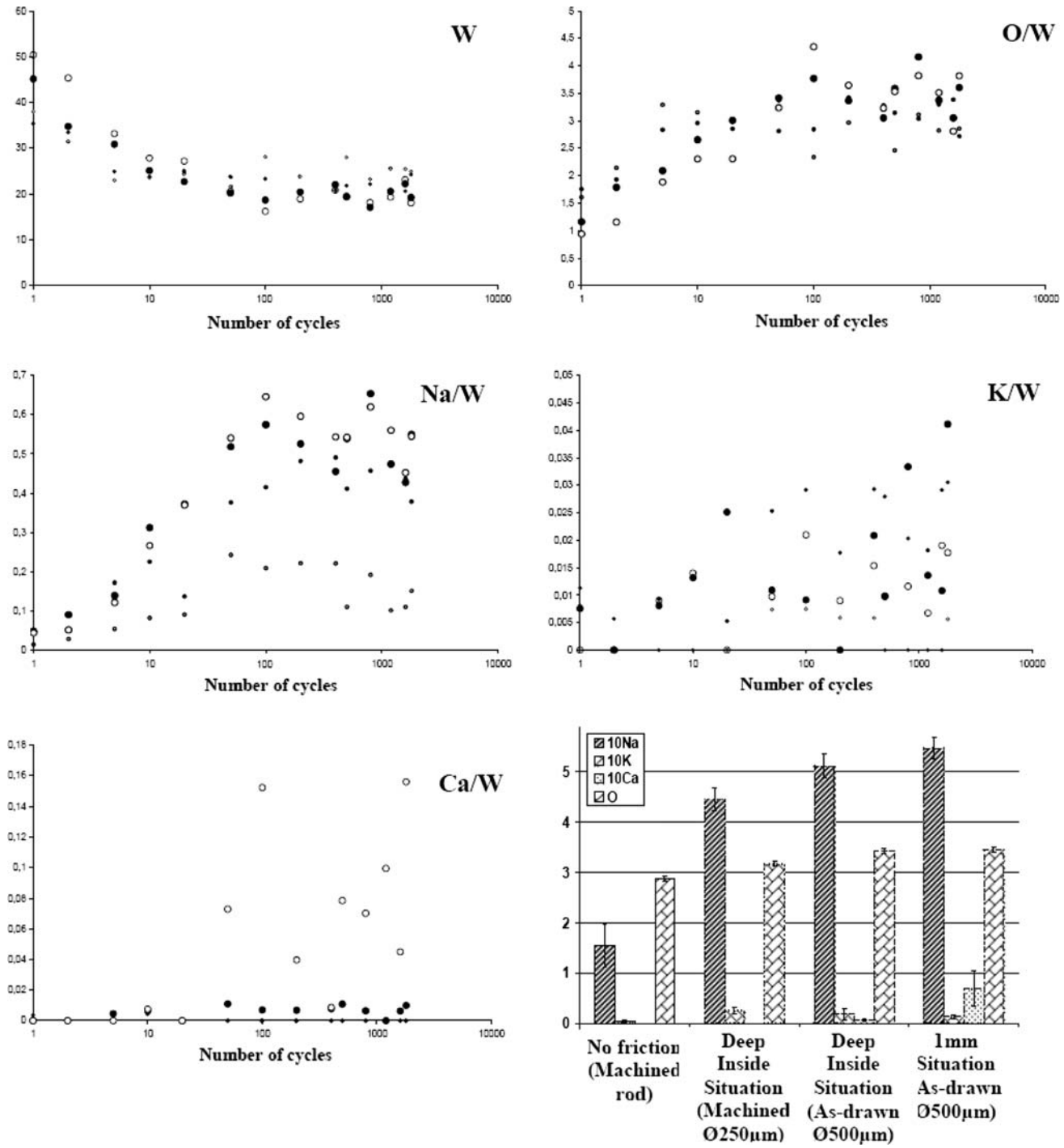

Fig. 6 EDX semi-quantitative analyses of the top of the oxide scale in the different situations after 1–1,800 cycles. The *small empty marks* refer to small-diameter "no friction situation", the *small full marks* to small-diameter "deep inside situation", the *large full marks* to large-diameter "deep inside situation", the *large empty marks* to large-diameter "1 mm situation". The values of the plateaus for Na/W, K/W, Ca/W, and O/W are summarized on the histogram

suggests the presence of tungstates and/or tungsten bronzes. In the "deep inside situation", the layer contains a large similar amount of Na and a small amount of K. The "1 mm situation" is characterized by a significantly higher amount of Ca.

Elementary analysis of the cross section of the scale

Elementary analysis of the cross section of the scale was performed with EDX for increasing numbers of thermo-mechanical cycles (Fig. 7). As in the top surface analyses,

Table 2 Composition of the oxides formed at the surface of the sample deduced from EDX semi-quantitative analysis, average values from 200 cycles to 1,800 cycles in the different situations, corresponding to the generic formula $Na_xK_yCa_zWO_i$

	No friction (machined rod)	Deep inside situation (machined Ø250 μm)	Deep inside situation (as-drawn Ø500 μm)	1 mm situation (as-drawn Ø500 μm)
x (Na)	0.15 ± 0.04	0.45 ± 0.02	0.51 ± 0.02	0.55 ± 0.02
y (K)	0.00 ± 0.00	0.02 ± 0.01	0.02 ± 0.01	0.01 ± 0.00
z (Ca)	0.00 ± 0.00	0.00 ± 0.00	0.01 ± 0.00	0.07 ± 0.03
i (O)	2.88 ± 0.05	3.17 ± 0.05	3.43 ± 0.05	3.45 ± 0.06

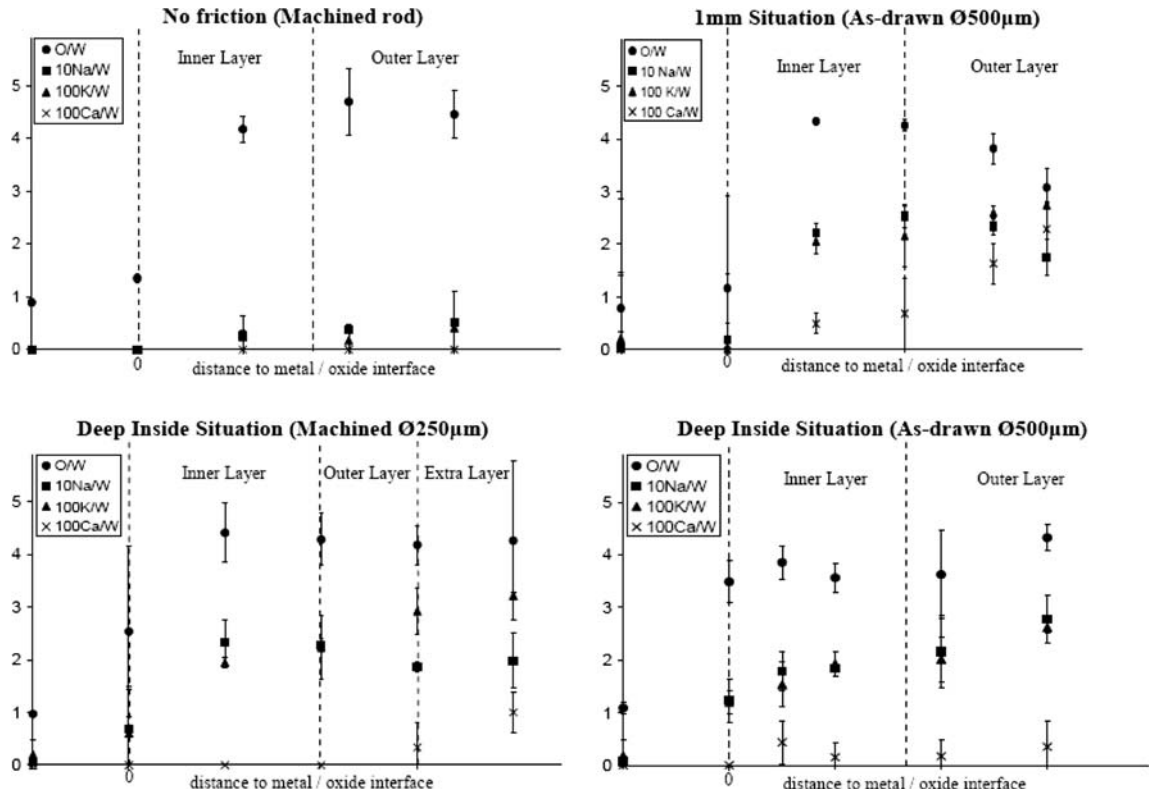

Fig. 7 Semi-quantitative composition profiles across the oxide scale of the different situations (IL, OL, and EL) after 1,800 cycles

the O/W ratio in the metallic zone is equal to 1 and is probably a semi-quantitative EDS artifact linked to tungsten absorbance.

There is no obvious discontinuity in the O/W ratio from one layer to another. The O/W ratio is falling near the inner layer–metal interface. In the inner layer, over the entire sample surface, Na and K are present in a ratio Na/W = 10 K/W. Since the ratio Na/K in the glass is not known, a correlation cannot be made with the inner layer. Na and K amounts are different in inner and outer layers, but no discontinuity is detected. Levels of Na and K are nearly the same in all friction situations but are slightly lower in the "no-friction" one.

Ca is not detected in the "no-friction" case and is present in the "1 mm situation" as expected from the top analyses. When present, Ca is in a higher level at the surface with a gradient perpendicular to the surface of the scale which leads to the conclusion that calcium is brought from the outside.

XRD analysis of the top of the scale

X-ray diffraction was performed on large-diameter samples that were used for 1,800 cycles for friction situations. Unused tungsten samples were used as a reference: all observed peaks were identified as tungsten ones, although complementary analysis using XPS has detected a thin oxide layer on the sample surface, as expected from literature [15]. The tungsten peaks were present on the diffractograms (Fig. 8). This suggests that

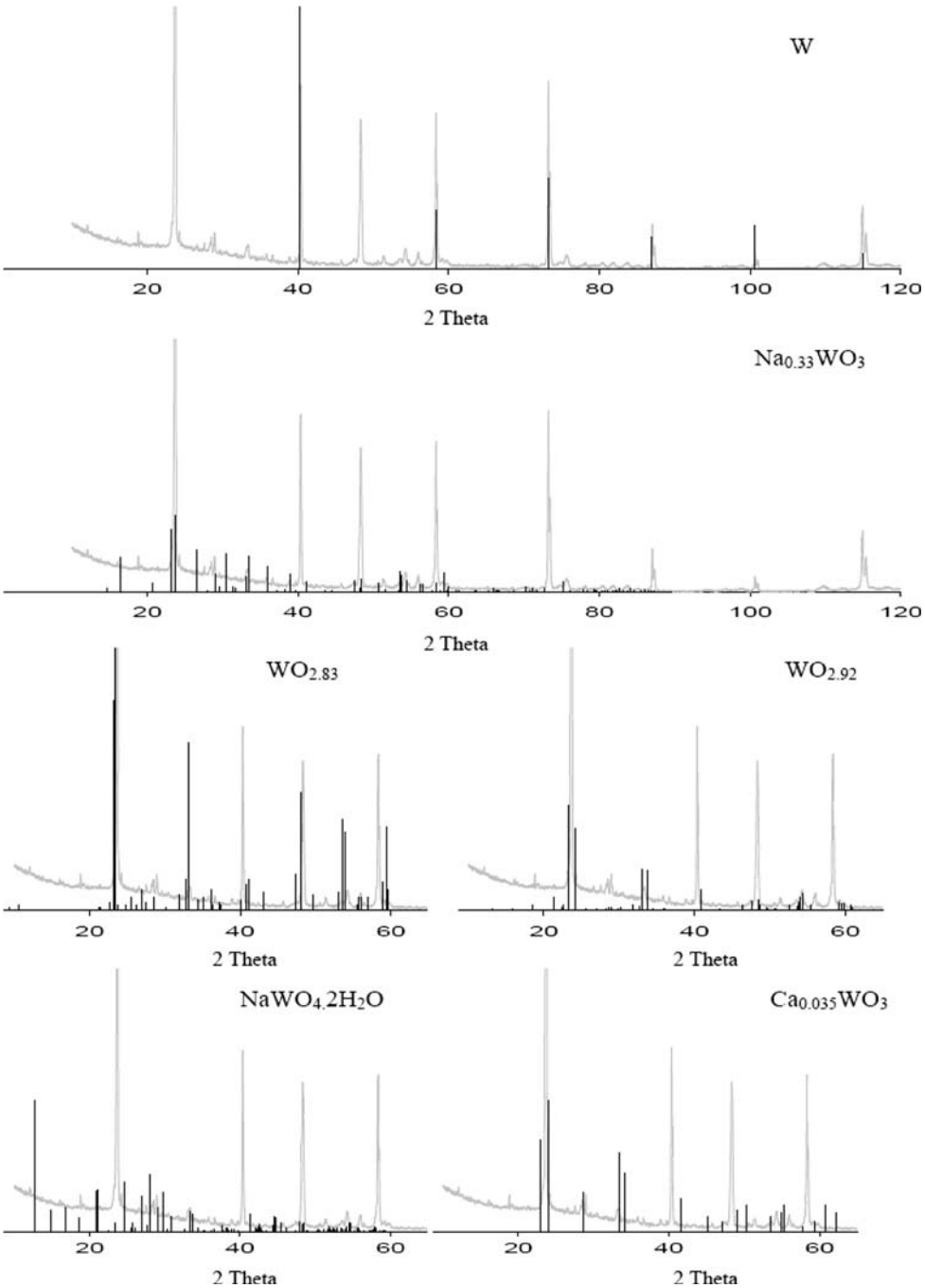

Fig. 8 X-ray diffractogram of the oxide scale on four samples of large-diameter samples after 1,800 cycles in the friction situations, put side by side to form a raft with a surface of 1 mm^2 limited to the 2Θ known zone of the references. The diffractogram is compared to expected peaks for tungsten and five tungsten-based oxides which significantly fit with experimental peaks

the underlying metal and the whole oxide scale were analyzed, despite the relatively thick oxide layer (typically 10 μm); an alternative possibility would be the (unobserved) presence of unoxidized W particles inside the scale.

As seen in Fig. 8, a large number of peaks are present on the diffractograms. Peak identification was attempted, on the basis of the expected oxide phases including the numerous tungsten bronzes referenced in literature that had the elements detected in the oxide scale: sodium, potassium, and calcium. The main peaks can be attributed to $Na_{0.33}WO_3$ [16], and $WO_{2.83}$ [17]. The other experimental peaks fit with many compounds, such as tungsten oxides ($WO_{2.92}$), tungsten bronzes ($Ca_{0.035}WO_3$), or hydrated tungstate ($NaWO_4{\cdot}2H_20$) as illustrated in Fig. 8.

Discussion

Experimental conditions in cyclic oxidation and wear of tungsten

Tungsten sample evolution is driven by three main conditions: chemical interactions, temperature amplitude, and friction.

- *Chemical interactions* are fixed by the phases in contact with the sample at a given time: air, hot glass, or "hot glass atmosphere". When tungsten, although not in contact with hot glass, is in a confined volume of air surrounded by hot glass, elements such as sodium or potassium evaporated from glass [18–20] can be present: we will refer to the resulting atmosphere as "hot glass atmosphere". In all cases, the sample is cooled in air. In the "no-friction situation", tungsten is heated in "hot glass atmosphere" during introduction in glass. In the other situations, tungsten is in a "hot glass atmosphere" until glass contact and when the sample is withdrawn.
- *Temperature amplitude* is determined by heat exchange with glass which is the only source of heat. In the "no-friction situation", tungsten is heated by radiative exchanges with glass and by conduction from the part of the sample immersed in glass. By contrast, in the "deep inside situation", tungsten is mainly heated by contact with hot glass. The average temperature reached for small diameter is expected to be higher than for large one because the surface to volume ratio is higher (smaller diameter). In the second part of the cycle, the sample is cooled down in air, so the situations with smaller diameter (whatever friction), reach a lower temperature more rapidly than the large diameter ones ("1 mm situation" and "deep inside situation"). As a consequence, the temperature amplitude is higher in the "deep inside situation" for small diameter than in the "no-friction situation" for small diameter and the "deep inside situation" for large diameter. As tungsten, in the "1 mm situation" experiments is heated later by glass, has a large diameter, and is in contact with the holder, it is expected to reach a lower temperature when heated and a higher temperature when cooled down. The temperature amplitude plays a role in the thermally activated mechanisms of oxidation and in the stresses between the oxide scale and the metal bulk of the sample induced by the differences in thermal expansion.
- *Friction* is due to the rotation between of the rod where tungsten and glass are in contact. In the small diameter "deep inside situation", the local friction rate is smaller than in large diameter "1 mm" and "deep inside" cases. The rod surface is also submitted to mechanical friction parallel to the sample axis, with the same velocity, for a short time when the rod is withdrawn from hot glass.

Tungsten oxidation mechanisms

The "no-friction situation" is essentially affected by high-temperature oxidation and is not concerned with rotational friction. As seen in Fig. 5, the growth of the oxide scale first obeys a classic parabolic-like law, which induces the increase in diameter of the rod during the first 50 cycles (Fig. 3). The growth is limited by diffusion through the scale, and the rate of formation of the scale is approximately inversely proportional to its thickness as assumed by Webb et al. [7] in the case of isothermal oxidation of tungsten in air between 700 and 1000 °C.

As mentioned in the literature [3–7], the scale is constituted by two layers. The inner layer progresses inside the metal, while the outer layer grows externally. The observation of the cross sections suggests a transformation at the interface between the two layers to form the grains of the outer layer. The observed grain size gradient can be explained by classic Ostwald ripening-like grain growth: the largest grains are the oldest ones, at the external surface of the scale.

The transformation at the inner–outer layers interface may involve the transformation from an oxide with lower oxygen content ($WO_{2.75}$ for instance), into a more oxygen-rich one (WO_3) [4, 6, 7]. This is consistent with a mechanism of oxygen diffusion as mentioned by Jepson and Aylmore [3] referring to results of Arkharov and Kozmanov [21]. The present situation differs from high-temperature oxidation of tungsten in air by the presence of sodium within the scale in the outer and the inner layers. Sodium could be brought by the "glass atmosphere" in the "no-friction situation" [18, 20]. The oxide average composition in this case, estimated from EDS analyses, is about $Na_{0.15}WO_3$. The corresponding phases are probably a mixture of bronzes and oxides; although, they could not be identified by XRD as these analyses were only carried on larger-diameter samples in friction situations. The crystallographic modifications from tungsten oxide to sodium bronze [22, 23] could also explain the shape of the grains as seen in Fig. 4.

As shown by the diameter decrease (Fig. 3), the growth of the scale, even in the "no-friction situation", is counterbalanced by erosion. Two main mechanisms may be responsible for this erosion. The first one is mechanical wear, which will be developed in the discussion for "friction situations". The second one is the volatilization of tungsten oxides [24] at the external surface. WO_3 for

instance is known to have significant volatilization rates when water vapour is present [9–11]. Water vapor was present, although not controlled, in the experiments. The volatilization mechanism could explain the flattened shape of the grains of the external pavement of the scale (Fig. 5). Whatever be the mechanism responsible for erosion, a steady state is expected to be reached, when the scale growth rate, which decreases as the scale grows, equals the erosion rate, which is mainly fixed by external conditions. This steady state in the oxide layer thickness corresponds to a linear decrease of the diameter with the number of cycles, which is observed in the apparent diameter variation (Fig. 3). Some cracks are also seen at the sample outer surface; they probably result from differential thermal expansion between the scale and the metallic bulk during thermal cycling. The cracks and the induced porosities could be a kinetic activator for oxidation.

Oxidation of tungsten coupled with friction

Friction with glass is an additional condition in the mechanism of tungsten oxidation when compared to the "no-friction situation".

The initial parabolic-like stage of the scale growth for the first 50 cycles is also observed (Fig. 3) in the "friction situations". The only noticeable difference is the lower rate of increase of the scale in the "1 mm situation", which can be explained by the already noticed lower temperature reached in this case in the hot stage. The scale formation mechanism described in the "no-friction case", which involves oxidation by atmospheric air, is also valid when friction operates, as an inner and an outer layers (Fig. 5) are observed. In "friction situations", some constitutive elements from the glass phase are detected in the oxide scale, but no evidence is found of a possible part played in the oxidation mechanism. However, they could induce, as already noticed in the case of sodium, some crystallographic transformations.

Although wear, due to friction with glass, is not directly involved in the layer growth, it has two consequences on the scale evolution:

- *Feed-back effect on oxidation* as the oxidation is limited by diffusion and almost inversely proportional to the scale thickness [7], the erosion of the outer layer by wear, which reduces the scale thickness, increases the oxidation rate. As already mentioned, the constant rate of diameter decrease corresponds to an oxide scale thickness at which the erosion rate equals the oxidation rate, leading to a steady state behavior in the oxide thickness.
- *Specific morphology of the outer layer of the scale* in the "deep inside situation" with small diameter, which corresponds to the higher rate of diameter decrease, the external grains of the outer layer are removed (or eroded) very rapidly, so they have no time to significantly grow, and almost no grain growth is observed. Slightly larger grains can be observed in the external part of the outer layer in the large diameter case in the same "deep inside situation". As a first approximation, the age of the outer grains, i.e., the time τ available for grain growth scales as the inverse of the erosion rate. On the basis of the decreasing slope of the curves in Fig. 3 indicating the erosion rate, if the "no-friction situation" is taken as unity, the large diameter "deep inside situation" is about 5, and the small diameter "deep inside situation" is about 10. In the "1 mm situation", which also corresponds to large diameter, erosion is only slightly higher than in the "no-friction one", and a noticeable grain growth is observed, together with a size gradient. In this case, the grains however remain much smaller: this is probably due to slower diffusion, owing to the lower temperature.

Although there is no direct observation of the wear mechanism, an important indication can be deduced from the difference of erosion rates depending on the wire diameter, i.e., on the linear velocity: the higher erosion rate is obtained with the smallest diameter, i.e., when the local friction velocity is smallest. To enable abrasion to be the dominant mechanism of wear, the friction velocity at the interface needs to be high, which is not the case here. With a slower friction velocity, the contact between the sliding solids is longer. As a result, an adhesive wear type of mechanism, involving physico-chemical interactions between glass and the oxide scale, is more likely to dominate the wear process, giving rise to most of the wear. Erosion in the "1 mm situation", lower than in the "deep inside one" for the same diameter, also presents an argument in favor of this adhesive-wear-type mechanism: the lower temperature in the "1 mm situation" reduces the thermally activated adhesion mechanisms, thereby allowing the oxide to be more easily detached from the tungsten rods.

Conclusion

The analyzed cyclic tungsten oxidation and wear in contact with glass and air atmosphere is controlled by local thermal conditions and geometric process factors. These conditions, which differ from one case to another, have been used in this article to evidence the main mechanisms involved in the complex overall phenomenon, and to outline their driving forces and kinetics.

When wear is not involved, the observed features are likely to result from a simple mechanism of oxidation

mainly influenced by diffusion. As in any oxidation process leading to a protective layer and controlled by diffusion, this rate is inversely proportional to the thickness. The particular shape of the objects forming the external layer brings to the hypothesis of tungsten oxides volatilization. The presence of sodium only influences the microstructure appearance of the oxides.

Friction with glass drives to an adhesive wear that influences oxidation. When the differential velocity between glass and tungsten is low (small diameter), glass adhesion is enhanced and wear is more important. As a result, the oxide thickness is lowered and then oxidation rate is increased. The decay in diameter of the rod is more rapid.

The temperature dependence of the oxidation rate has been checked. This cyclic oxidation also leads to cracks, independent on glass contact and likely due to cyclic thermal expansion stresses.

Complementary studies are in progress to improve the scale characterization and to quantitatively model the phenomena.

References

1. Lassner E, Schubert W-D (1999) Tungsten, properties, chemistry, technology of the element alloys and chemical compounds. Kluwer Academic/Plenum Publishers, New York
2. Yih SWH, Wang CT (1979) Tungsten sources, metallurgy properties and applications. Plenum Press, New York
3. Jepson WB, Aylmore DW (1961) J Electrochem Soc 108(10):942
4. Gulbransen EA, Andrew KF (1960) J Electrochem Soc 107(7):619
5. Kellett EA, Rogers SE (1963) J Electrochem Soc 110(6):502
6. Ong JN Jr (1962) J Electrochem Soc 109(4):284
7. Webb WW, Norton JT, Wagner C (1956) J Electrochem Soc 103(2):107
8. Baur JP, Bridges DW, Fassell WM (1956) J Electrochem Soc 103(5):266
9. Smolik GR, Pawelko RJ, Anderl RA, Petti DA (2001) Fusion Eng Des 54:583
10. Greene GA, Finfrock CC (2001) Exp Thermal Fluid Sci 25:87
11. Greene GA, Finfrock CC (2002) Exp Thermal Fluid Sci 26:917
12. Adib Hajbagheri F, Kashani Bozorg SF, Amadeh AA (2008) J Mater Sci 43:5720. doi:10.1007/s10853-008-2890-9
13. Gialanella S, Ischia G, Straffelini G (2008) J Mater Sci 43:1701. doi:10.1007/s10853-007-2358-3
14. Zhang XP, Zhao ZP, Wu FM, Wang YL, Wu J (2007) J Mater Sci 42:8523. doi:10.1007/s10853-007-1738-z
15. Musket RG (1970) J Less-Common Met 22:175
16. Takusagawa F, Jacobson RA (1976) J Solid State Chem 18:2163
17. Booth J, Ekstörn T, Iguchi E, Tilley RTD (1982) J Solid State Chem 41:293
18. Ledieu A (2004) Altération par l'eau des verres borosilicates: expériences, modélisation et simulations Monte Carlo, Thesis, Palaiseau, p 26
19. Van Limpt H, Beerkens R, Verheijen O (2006) J Am Ceramic Soc 89(11):3446
20. Yu Y, Hewins RH, Alexander CMO'D, Wang J (2003) Geochim Cosmochim Acta 67(4):773
21. Arkharov VI, Kozmanov Yu D (1957) Akad Nauk SSSR 2:131
22. Rosen C, Post B, Banks E (1956) Acta Cryst 9:477
23. Wang J, Liu G, Du Y (2003) Mater Lett 57:3648–3652
24. Blackburn PE, Hoch M, Johnston HL (1958) J Phys Chem 62(7):769